Correlation of Structural and Electronic Properties with Solar Cell Efficiency for Amorphous Silicon Deposited at Increasing Growth Rates

G. Ganguly[1], D. Han[2], D.L. Williamson[3], B.P. Nelson[4] and J. D. Cohen[5]
[1] BP Solar, Toano, VA; [2] University of North Carolina, Chapel Hill, NC; [3] Colorado School of Mines, Golden, CO; [4] NREL, Golden, CO; [5]University of Oregon, Eugene, OR

ABSTRACT

This paper details the effects of increasing the growth rate of hydrogenated amorphous silicon (a-Si:H), deposited by dc plasma chemical vapor deposition, on the structural and electronic properties of the material in comparison with the performance of solar cells incorporating such layers. The hydrogen content exhibits the strongest correlation with the solar cell efficiency. The defect density measured by two different techniques, correlate poorly but when measured by a third technique, correlates well. On the other hand, the Urbach tail slope correlated well when measured by two different techniques but poorly when measured by a third one.

1. Introduction

This study involving several groups in the amorphous silicon team was an attempt to discern the dominant changes occurring when the a-Si:H i-layers are deposited at increasing rates from 1 to 10Å/s. While several studies have focused on the variation of material properties with growth rate, we have attempted to find the relative importance of each characteristic by attempting a large set of measurements on a large set of co-deposited samples.

2. Sample Preparation

All samples were deposited by dc plasma decomposition of silane and hydrogen onto different substrates in a single run. These are

(a) Crystalline silicon (c-Si) for Fourier transform infrared spectroscopy (FTIR) to obtain the H-bonding configuration and H-content;

(b) High purity, low Fe content Al foil for small angle X-ray scattering (SAXS) to obtain the void distributions

(c) Consumer grade Al foil for floatation measurements of the film density;

(d) Corning 1737F glass with pre-deposited, coplanar Cr contacts for measurements of the defect density (N_d) and Urbach energy (E_u) by the constant photocurrent method (CPM);

(e) Chemically frosted, Corning 1737F glass for photoluminescence (PL) measurements.

(f) ZnO coated glass substrates for drive-level profiling (DLCP) method of obtaining defect density as well as transient photocapacitance (TPC) spectroscopy to obtain Urbach tail slopes.

The solar cells were deposited on smooth SnO_2 coated glass in independent runs. Some samples were light soaked for 600h at ~50°C under 1sun illumination from Na vapor lamps.

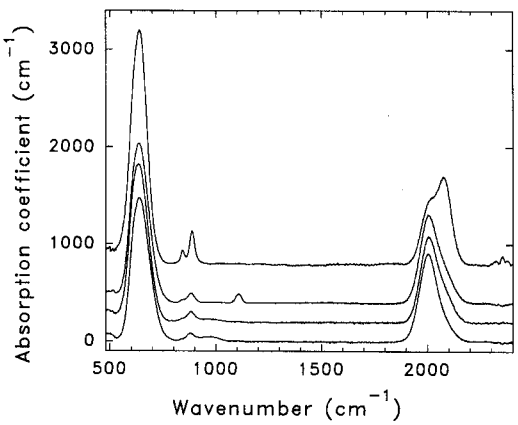

Fig. 1. The infrared absorption spectra displaced upwards with increasing growth rate.

3. IR and ρ

The infrared absorption spectra for the four samples are shown in Fig. 1. Clearly, with increasing deposition rate, there is a systematic increase in the absorption in the 840-900cm^{-1} region indicating an increased multi-hydride type bonding. At the same time, the stretching vibrational modes in the 2000cm-1 region indicates relatively more absorption on the higher wave number side of the band. The hydrogen content and the value of the structure factor, 'R' is tabulated in Table I. Both quantities increase with increasing deposition rate. The density (ρ±0.01 g/cm^3) was measured on films remaining after the Al foil substrate is etched away from the a-Si:H in an HCl solution by putting into a BaCl solution of varying density until it is suspended. The values are shown in Table I and decrease with increasing deposition rate.

Table I. A summary of properties

Sample	Dep. Rate (Å/s)	[H] (at.%)	R	ρ (g/cm^3)	f (vol.%)
L2127	1	10.4	0.16	2.22	0.02
L2129	3	11.6	0.24		0.08
L2136	5	12.2	0.24	2.20	0.08
L2137	10	16.1	0.60	2.13	0.6

4. SAXS

The SAXS data of the samples are shown in Fig. 2. One can see a trend of increasing SAXS with deposition rate. A large increase in scattering is seen for the highest deposition rate. The integrated SAXS is used to estimate the microvoid fraction, f, which is quite low up to a growth rate of 5A/s but then increases sharply for the 10Å/s material (Table I).

The latter result is consistent with the large increase in the IR microstructure factor, R for this sample. The sizes of the scattering features were obtained by fitting a distribution of spheres. The distributions are somewhat skewed. The sample L2137 was also examined by SAXS in the tilted mode and a modest change was observed, consistent with slightly elongated objects along the growth direction. A correction to the void fraction was made based on an ellipsoidal model. The diffuse scattering component in the SAXS, I_D, is related to the level approached at high q, and is correlated with the H content. It can only be roughly estimated for the highest growth rate material due to the significant scattering at the highest q caused by the very small scattering objects, D ~ 1 nm. All the data suggest a consistent picture of the microstructure of the four samples.

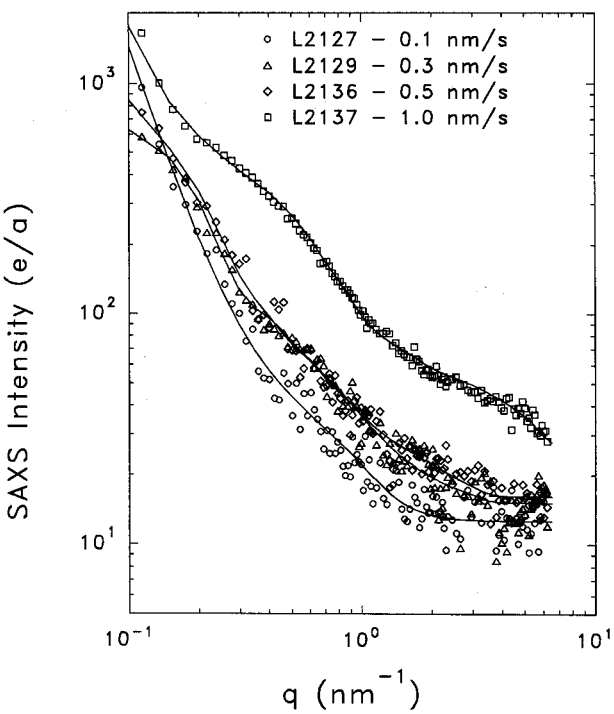

Fig. 2. The SAXS scattering intensity

5. PL

The PL spectra at low temperatures (T < 150 K) are dominated by the tail-to-tail, radiative transitions that yield the PL main band at ~1.4eV. The low energy defect PL band at ~0.88eV is relatively weak and can be measured at higher temperatures. In order to extract the information of the electronic tail states and the dangling bond states, all the PL spectra were deconvoluted into components at 80K. The integrated intensity, I_{main}, is plotted as a function of temperature in Fig. 3. One can see weaker temperature dependence with increasing growth rate suggesting a wider band tail. The defect band intensity is observed to increase with growth rate in the as deposited (A) and light soaked (B) states, as shown in Fig. 4.

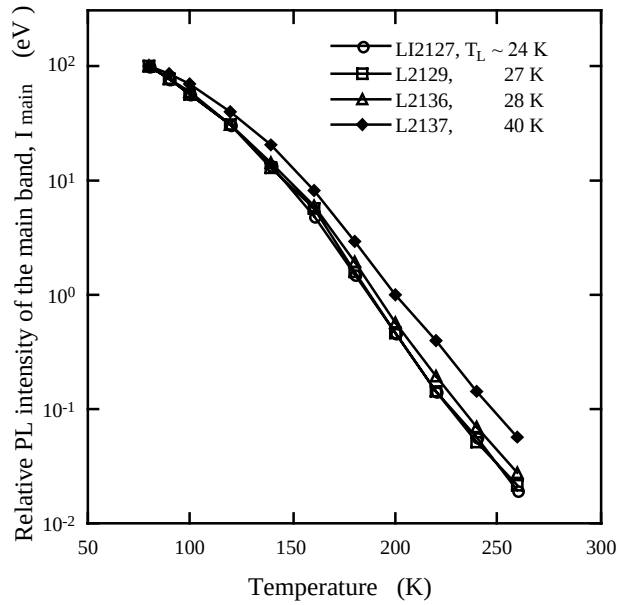

Fig. 3 The temperature dependence of the main PL band

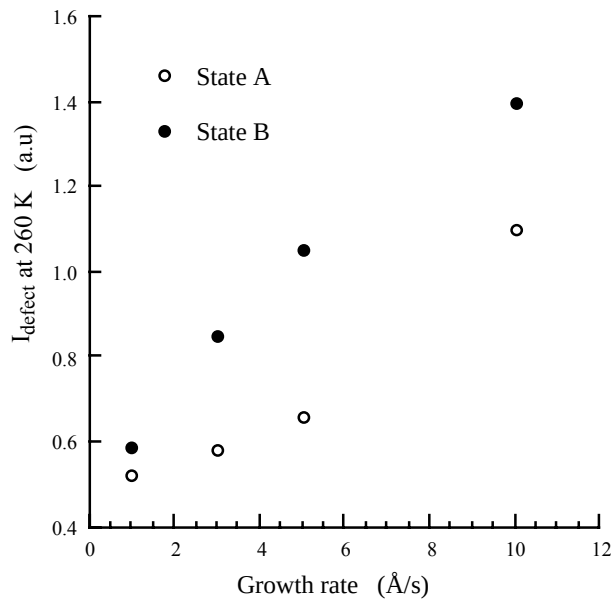

Fig. 4 The intensity of the defect PL band in annealed (A) and light soaked (B) states

6. CPM

The defect density and slope of the Urbach absorption tail obtained from CPM measurements are shown in Table II. There does not appear to be a clear trend for either quantity with increasing film growth rate – although the data for the highest growth rate is missing.

Table II Parameters obtained from CPM measurements

Sample	Dep.Rate (Å/s)	CPM Defect Density (cm^{-3})	Urbach Slope (meV)
L2127	1	4.20x10^{16}	61
L2129	3	4.26x10^{16}	57
L2136	5	5.38x10^{16}	63
L2137	10	-	-

7. Solar Cell Efficiency

There is a gradual, monotonic decrease of the solar cell efficiency with increasing growth rate as shown in Fig. 5.

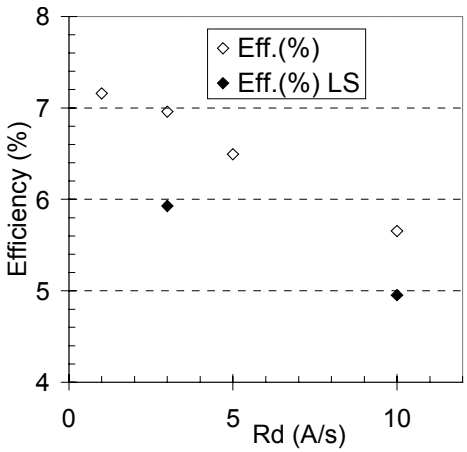

Fig. 5 The efficiency of solar cells deposited at different growth rates in the initial and 600h light soaked states

8. DLCP and TPC

We determined the deep defect densities for this series of samples using the DLCP method. Fig. 6 shows *no correlation* between the defect densities in these samples for either state A or state B and the growth rate (and hence neither with the device performance).

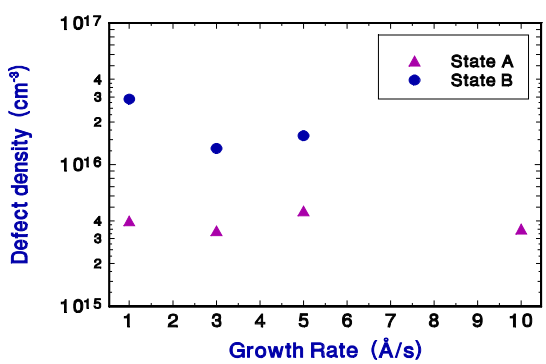

Fig. 6 The DLCP measured deep defect density in the as deposited (A) and light soaked (B) states.

We also characterized these films using TPC spectroscopy. The TPC technique essentially yields an optical absorption spectrum with a very high sensitivity. TPC spectra for both the lowest and highest growth rate samples in State A are shown in Fig. 7. Such spectra are well fit using a combination of a gaussian band of deep defects plus an exponential band of tail states. For this series of samples we found, in agreement with our results on an earlier sample series, that the Urbach energies determined were correlated with growth rate such that higher growth rates exhibited broader band tails.

9. Correlations

We compared the degree of correlation between each material property and the cell efficiency as shown in

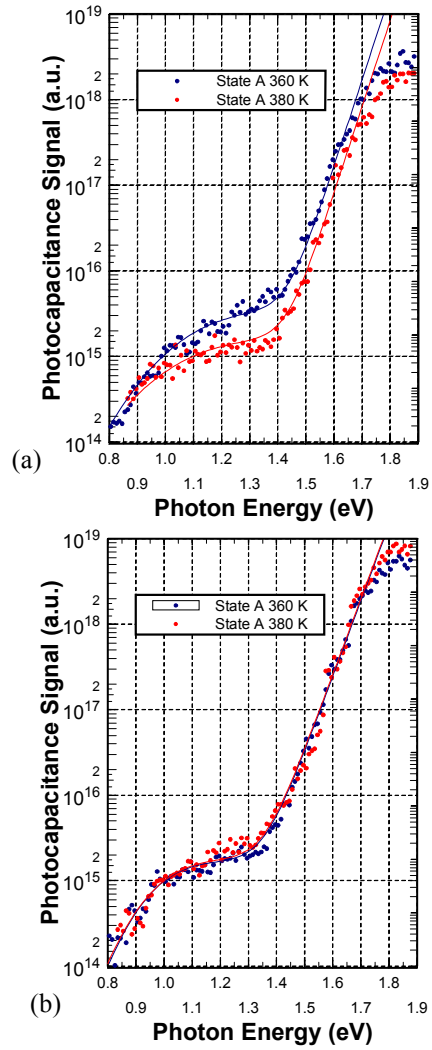

Fig. 7. The TPC measured sub-band gap spectra in the a-Si:H films deposited at (a) 1 and (b) 10Å/s

Fig. 8. The best correlation is observed with the hydrogen content (0.97) with improved correlation (0.99) when the efficiency is replaced with short circuit current density. There is also a good correlation with the diffuse SAXS scattering intensity, I_d (0.95), which is related to the hydrogen content. These suggest that widening of the band gap is the primary effect. Reasonable correlation is observed with the PL defect band intensity (0.96) but not with the DLCP defect density. The Urbach tail slope exhibits good correlation when determined from the temperature dependence of the PL main band (0.94) or TPC spectra (0.95) but not CPM. This suggests that low temperature processes through the band tail as well as mid-gap defects are somehow related to recombination processes in a solar cell at room temperature. However, not all techniques measure the same set of 'deep' or 'tail' defects. Finally, there is some correlation with the flotation density (0.94), microstructure factor, R (0.90) and CPM defect density (0.91). This approach can be used with other deposition parameters to identify useful material characterization tools.

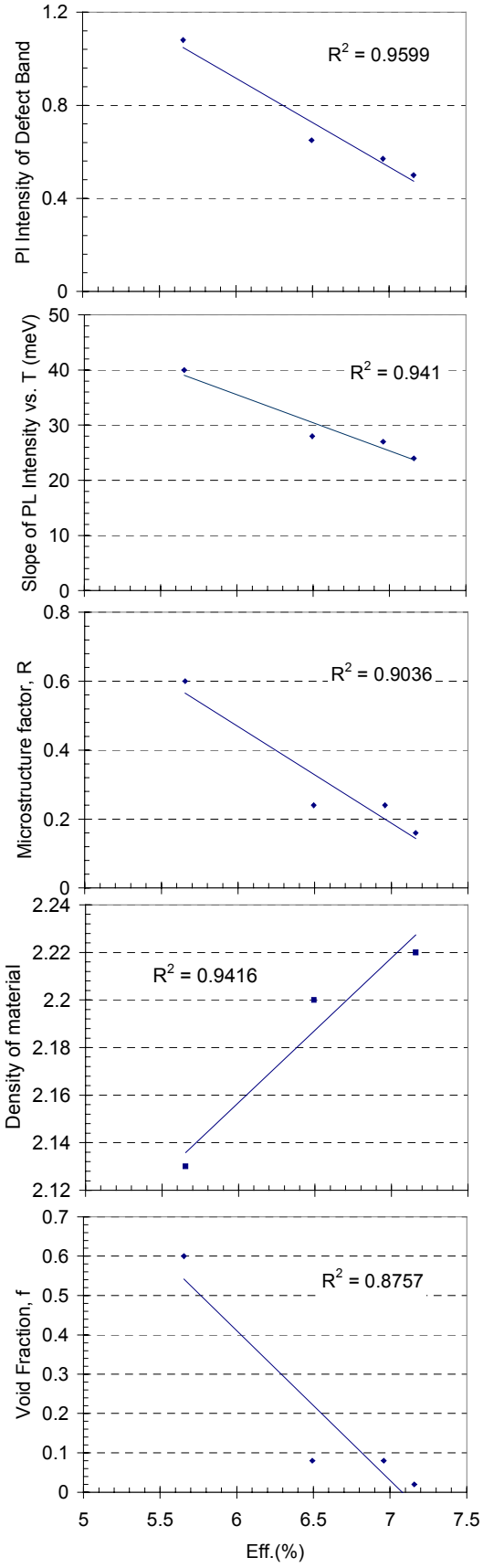

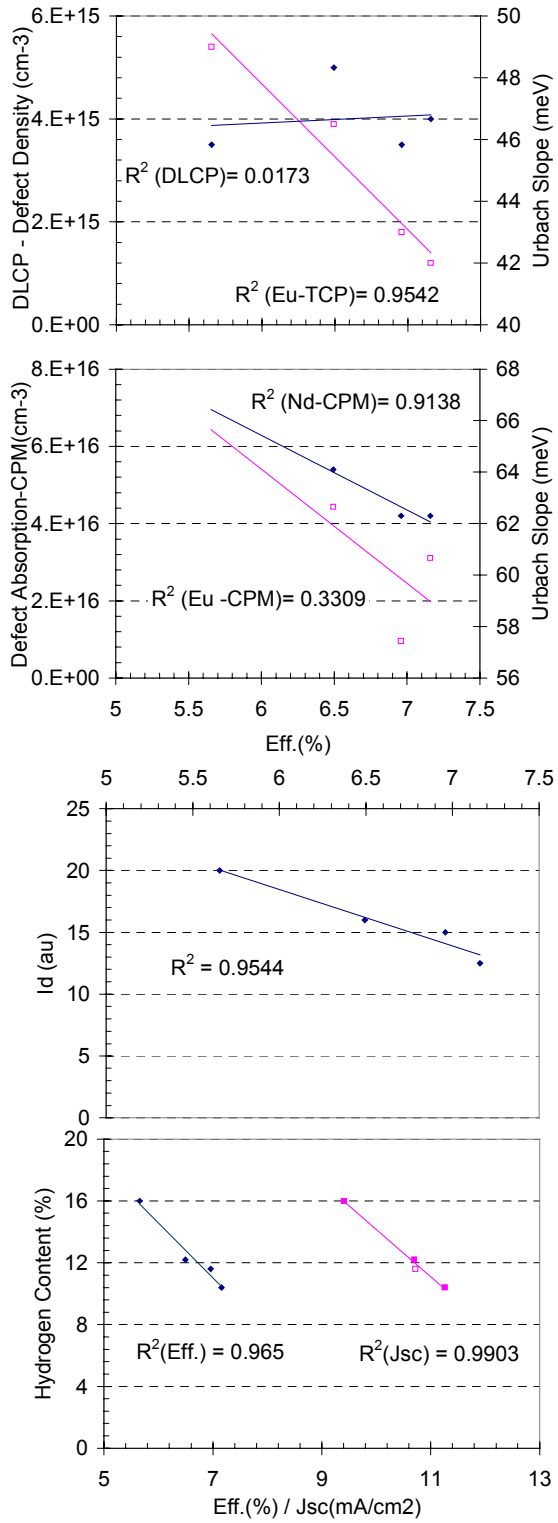

Fig. 8 Correlation of various material properties with the corresponding cell efficiencies and/ or short circuit current.

10. Acknowledgements

This work was supported by NREL subcontracts ZDJ-2-30630-10 (BPS), ADJ-1-30630-09 (UNC), XDJ-2-30630-27 (CSM) and ADJ-2-30630-17 (UO). We would like to thank Lynn Gedvilas (FTIR) and Yueqin Xu (CPM) at NREL for their contribution.